Laminar natural convection in shallow air rectangular cavities

Samy M. ElSherbiny
Mechanical Eng. Dept., Faculty of Eng., Alexandria University, Alexandria, Egypt

The laminar natural convection in shallow inclined air rectangular cavities is studied both numerically and experimentally. The effects of side walls thermal boundary conditions; aspect ratio, *A*; Rayleigh number, *Ra* and angle of inclination, φ on the flow and heat transfer characteristics are investigated. The two-dimensional governing equations for mass, momentum and energy conservation are solved using an implicit finite-difference scheme. Streamlines and isotherms as well as temperature and velocity distributions at different *Ra*, *A*, φ and side walls boundary conditions are shown in order to explain the flow and heat transfer characteristics. The case of perfectly conducting side walls gave lower heat transfer than that of the perfectly insulating side walls. The average Nusselt number showed a strong dependence on the system parameters: *Ra*, A and φ. New experimental data are presented for a square air cavity with perfectly conducting side walls which cover vertical and inclined layers for *Ra* up to 1.7×10^8. The present numerical and experimental results are in excellent agreement with previous data.

يقدم البحث دراسة عملية وعددية للحمل الحر داخل حيز مملوء بالهواء مقطعه على هيئة مستطيل. أحد الأسطح ساخن عند درجة حرارة ثابتة والسطح المقابل له بارد. السطحان الأخران من مادة اما موصلة تامة للحرارة أو عازلة لها تماما. وقد غطت الدراسة مدى كبير من رقم رالى من ١٠ ^٢ الى ١,٧ ×١٠ ^٨ وزاوية ميل من صفر(تسخين من أسفل) الى ١٨٠ ° (تسخين من أعلى) وذلك لحيز له نسبة أبعاد ١ أو ٠,٥ وقدم البحث أشكال توزيع خطوط السريان ودرجات الحرارة والسرعة لحالات مختلفة لتوضيح خواص السريان وأنتقال الحرارة. وقد أظهرت النتائج توافقا تاما بين النتائج العددية والعملية الحالية مع النتائج المنشورة من أبحاث أخرى.

Keywords: Natural convection, Rectangular cavities, Shallow layers, Square enclosures.

1. Introduction

The natural convective flow and heat transfer in a rectangular cavity is a simple model of considerable practical interest. The best known application is the double glazed windows. Other applications include reactor insulation, cooling of radioactive waste containers, ventilation of rooms, fire prevention, solar energy collection, dispersion of waste heat in estuaries and crystal growth in liquid metals. There are numerous studies regarding natural convection in enclosures. A review of the literature is given by Ostrach [1] and Raithby and Hollands [2].

Dimensional analysis shows that the flow and heat transfer within the rectangular layer (fig. 1) depend on each of the aspect ratio, A; the Rayleigh number, *Ra*; the Prandtl number, *Pr*; the angle of inclination, φ and the side walls boundary conditions. Most of the work is related to either side or bottom heating. However, heating from the side and cooling from the top was also investigated [3]. Numerical and experimental studies were concerned with rectangular layers with moderate or high aspect ratio (*A*>1) [4-8]. Other studies were devoted to shallow cavities with (*A*<1) [9-16]. The stability of the natural convective flow was studied by Hollands et al [4] and Catton [17]. Also, Roux et al. [11] performed a numerical study for air at $A = 1$ and $\varphi = 90°$ in the range $10^2 \le Ra \le 10^5$ to determine the limits of the conduction and boundary layer regimes. For the case of Linear Temperature Profile (LTP) on the side walls and $Ra < 10^3$, the conduction regime prevails while the laminar boundary layer regime starts at $Ra = 8500$. Experiments for the natural convection heat transfer in enclosures of moderate aspect ratios were performed by Meyer et al. [12] using an interferometric technique. The results covered the range of $Ra \le 7\times10^4$ and $0.25 \le A \le 4$. They found that the

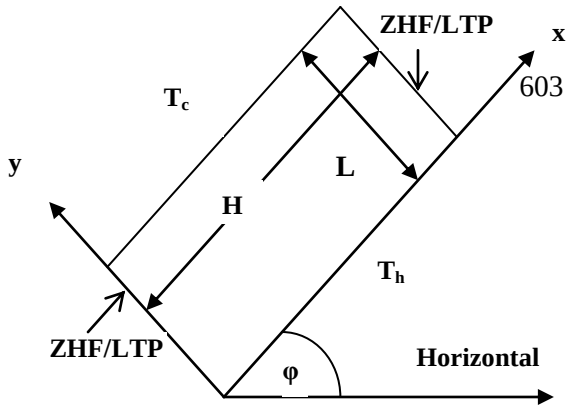

Alexandria Engineering Journal, Vol. 43 (2004), No. 5, 603-613

Fig. 1. The inclined rectangular cavity.

heat transfer is a strong function of the aspect ratio for A<4.

An experimental study on the effects of the thermal boundary conditions of the side walls on the natural convection within the enclosure was given by ElSherbiny et al. [18] for $A \geq 5$. Meyer et al. [13] studied the same effects both numerically and experimentally for $0.5 \leq A \leq 1$ and $Ra \leq 10^5$. The results showed that Nusselt numbers for Zero Heat Flux (ZHF) on the side walls are substantially higher than those for LTP. Koutsoheras and Charters [10] studied numerically the effect of side wall boundary conditions for air layers in the range $0.33 \leq A \leq 3$. They found that LTP can be represented if the ratio of wall material conductivity to the fluid thermal conductivity (k_w/k) is higher than 10. For perfectly insulated side walls, this ratio should be less than 0.05. Catton et al. [9] studied the effect of tilt angle on Nu for low A and both types of boundary conditions. Their results for a vertical air layer showed that the Nusselt number for LTP is lower than that for ZHF. However, this effect becomes more pronounced for lower aspect ratios (A<1).

A benchmark solution for A = 1, φ = 90° and ZHF was given by DeVahl Davis [14] for air (Pr = 0.71). It is believed to give the most accurate results for this special case. He used second-order, central difference approximations for all space derivatives. Mesh refinement and extrapolation of the results led to solutions for $10^3 \leq Ra \leq 10^6$ with high accuracy. Kuyper et al. [10] presented numerical simulations for inclined air cavities for both laminar and turbulent flows. The results covered the range $10^4 \leq Ra \leq 10^{11}$ for $0 \leq \varphi \leq 180°$ and the Nusselt number showed strong dependence on φ and Ra.

2. Theoretical analysis

The two-dimensional rectangular air layer and the Cartesian coordinate system are shown in fig. 1. One surface is isothermally heated at T_h and the opposite one is isothermally cooled at T_c. Two different side wall thermal boundary conditions, namely that of ZHF and LTP are investigated for being the two extremes of any real case. The first represents perfectly insulating side walls while the second represents infinitely conducting side walls. The angle of inclination, φ is measured in the anti-clockwise direction with φ = 0 is the horizontal layer heated from below. The Boussinesq approximation is adopted. That is, the physical properties and the density are assumed constant except in the buoyancy term.

2.1. Governing equations

The dimensionless equations governing the flow and heat transfer at steady state are given as follows:

$$\frac{\partial U}{\partial X}+\frac{\partial V}{\partial Y}=0. \tag{1}$$

$$U\frac{\partial U}{\partial X}+V\frac{\partial U}{\partial Y}=-\frac{\partial P_d}{\partial X}+Pr\left(\frac{\partial^2 U}{\partial X^2}+\frac{\partial^2 U}{\partial Y^2}\right) + Ra.Pr.(\theta-1)Sin\phi \tag{2}$$

$$U\frac{\partial V}{\partial X}+V\frac{\partial V}{\partial Y}=-\frac{\partial P_d}{\partial Y}+Pr\left(\frac{\partial^2 V}{\partial X^2}+\frac{\partial^2 V}{\partial Y^2}\right) + Ra.Pr.(\theta-1)\,Cos\phi \tag{3}$$

$$U\frac{\partial \theta}{\partial X}+V\frac{\partial \theta}{\partial Y}=\frac{\partial^2 \theta}{\partial X^2}+\frac{\partial^2 \theta}{\partial Y^2}. \tag{4}$$

Where,

$$U=\frac{u}{\alpha/L},\quad V=\frac{v}{\alpha/L},\quad X = x/L,\quad Y = y/L,$$

$$P_d=\frac{p_d}{\rho\alpha^2/L^2}$$

$$\theta = \frac{T - T_c}{T_h - T_c},\ Ra = \frac{\beta g (T_h - T_c) L^3}{\nu \alpha},\ Pr = C_p \mu / k,$$

$$Gr = \frac{\beta g (T_h - T_c) L^3}{\nu^2}$$

2.2. Boundary conditions

The governing equations are subject to the following boundary conditions:

at $Y = 0,\ 0 \le X \le A$: $U = 0,\ V = 0,\ \theta = 1$;

at $Y = 1,\ 0 \le X \le A$: $U = 0,\ V = 0,\ \theta = 0$;

at $X = 0,\ 0 \le Y \le 1$: $U = 0,\ V = 0,\ \frac{\partial \theta}{\partial X} = 0$ (for ZHF) *or* $\theta = 1 - Y$ (for LTP);

at $X = A,\ 0 \le Y \le 1$: $U = 0,\ V = 0,\ \frac{\partial \theta}{\partial X} = 0$ (for ZHF) *or* $\theta = 1 - Y$ (for LTP).

A (the cavity aspect ratio) = plate height / plate spacing = H / L.

2.3. Local and average Nusselt numbers

The local Nusselt number at any point on the hot surface, Nu_x is defined as:

$$Nu_x = \frac{h_x L}{k} = -\frac{\partial \theta}{\partial Y} \ (at\ Y = 0), \qquad (5)$$

, and the average Nusselt number over the hot surface, Nu is calculated as:

$$Nu = \frac{h L}{k} = -\frac{1}{A} \int_0^A \frac{\partial \theta}{\partial Y}\, dX \ (at\ Y = 0). \qquad (6)$$

2.4. Numerical procedure

The equations are expressed in finite difference form using central differences and are successively iterated from some arbitrary initial conditions (stagnant conditions) until steady-state conditions are reached. The resulting finite difference equations were solved using the SIMPLER technique developed by Patankar [19] with an Alternating-Direction Implicit (ADI) algorithm. The Nusselt number is then calculated using the converged solution for temperature field. A grid independence study is conducted using four different grid sizes with 21×21, 31×31, 41×41, and 51×51 nodes. It was shown that a further refinement of grids does not have any significant effect on the average Nusselt number. Therefore, a non-uniform grid of 51×51 points is used for all calculations. The non-uniform mesh is used to better resolve the thin thermal boundary layer associated with high Rayleigh numbers.

3. Experimental setup

A new method of measuring surface heat flux was used. The method, as shown in fig. 12, uses Peltier cooling or heating to bring the temperature of a special plate (cap) embedded in the surface to the surface temperature to maintain an isothermal surface. The experimental apparatus, developed and previously used by Shewen [20], consists of two plates each one was machined from aluminum slab of 28 mm thick and measured 850mm wide by 750 mm high. Each plate contained five Peltier-effect Heat Flux Meters (PHFM) positioned along the vertical centerline. Each PHFM used nine Thermo-Electric Modules (TEM) arranged in a 3×3 array. These are inserted in the plate recess and covered by a metallic cap made of copper. A cross-sectional view of a PHFM is shown in fig. 12. The cap is flush with the surrounding plate surface and serves primarily to ensure a uniform surface temperature. Each thermo-electric module contains 31 P/N couples of semiconductor rods arranged electrically in series and thermally in parallel. The voltage of the TEM is proportional to the temperature difference across the P/N junctions. The PHFM has the ability to transfer heat across the cap under an applied direct electric current. The direction of heat flux depends on the current polarity. Thermocouples are embedded in both of the cap and the aluminum plate to measure the temperature difference.

Each plate temperature was maintained by circulating water from a constant temperature bath through an array of tubes attached to the

rear surface of the plate. The two plates were supported by a portable rack which facilitated the adjustment of plate spacing, L and provided for the rotation about a horizontal axis by ± 95° of vertical position. The two plates are inserted inside a horizontal cylindrical pressure vessel where the air pressure can be varied from 1 Pa to 1140 kPa absolute. Thus, the Rayleigh number can be varied over 12 orders of magnitude. The rear of each plate was thermally insulated using a 60 mm thick layer of fiber glass insulation to reduce the rear heat losses. The perfectly conducting side walls were achieved by using 6.4mm steel plates fixed between the aluminum plates. A thin layer of silver paste of a high thermal conductivity was applied at the aluminum/ steel interface to reduce the thermal contact resistance. Eleven thermocouples attached at even locations along the side walls assured the LTP between the two isothermal aluminum plates.

4. Numerical results

The present computations are carried out for air with $Pr = 0.71$. The effect of aspect ratio is studied for a square cavity ($A = 1$) and a shallow cavity of $A = 1/2$. The effect of Ra is numerically investigated in the range $10^2 \le Ra \le 10^6$ and the angle of inclination was varied from heating from below ($\varphi = 0$) to heating from above ($\varphi = 180°$). The two different extremes of boundary conditions (ZHF and LTP) were also examined.

4.1. Flow patterns

The streamlines and isotherms for a vertical square air layer with ZHF on the side walls are shown in fig. 2. For $Ra = 10^3$, a weak stable unicellular flow fills the cavity indicating the conduction regime. The isotherms are slightly distorted and symmetry is noticed about the center of the cavity. The isotherms are slightly closer at the lower end of the hot surface than at the upper end. For $Ra = 10^6$, the boundary layer type of flow exists at the hot and cold surfaces. A large temperature gradient is shown near the bottom of the hot surface and the top of the cold one. A uniform vertical temperature gradient is shown at the vertical centerline of the cavity.

The effects of changing the boundary conditions and angle of tilt on the flow patterns are shown in fig. 3 for $\varphi = 60°$ and LTP. For $Ra = 10^3$, the heat transfer is governed by conduction with lower Nu for LTP than for ZHF. For $Ra = 10^6$, the location of the maximum Nu_x moved up from the lower end of the hot surface.

The effects of lowering the aspect ratio to $A = 1/2$ are shown in figs. 4 and 5. For a vertical air layer with ZHF, fig. 4 shows the same trends in streamlines as those for $A = 1$. However, for $A = 1/2$, the effect of side wall conductance is more pronounced and lower Nusselt numbers than for $A = 1$ are expected. For $\varphi = 120°$ (heated from above), fig. 5 shows more stable flows and lower Nu than for $\varphi = 90°$.

4.2. Effect of side walls

The effect of side walls boundary conditions on Nu at different Ra is shown in fig. 6 for $A = 1$ and $\varphi = 90°$. The LTP gives lower heat transfer than the ZHF boundary conditions. The difference in Nu between the two cases increases with Ra. A comparison with previous data from other authors shows an excellent agreement.

4.3. Effect of inclination

The present numerical results for the average Nusselt number in the range $10^3 \le Ra \le 10^6$, $0 \le \varphi \le 180°$ and for ZHF and LTP are plotted in fig. 7 for $A = 1$ and fig. 8 for $A = 1/2$.

The results show a strong dependence on φ and Ra. Heating from below ($\varphi < 90°$) always gives higher heat transfer than heating from above ($\varphi > 90°$). The maximum Nu occurs at an angle between 60° and 90°, depending on Ra. Decreasing the aspect ratio from 1 to 1/2 caused a decrease in Nu.

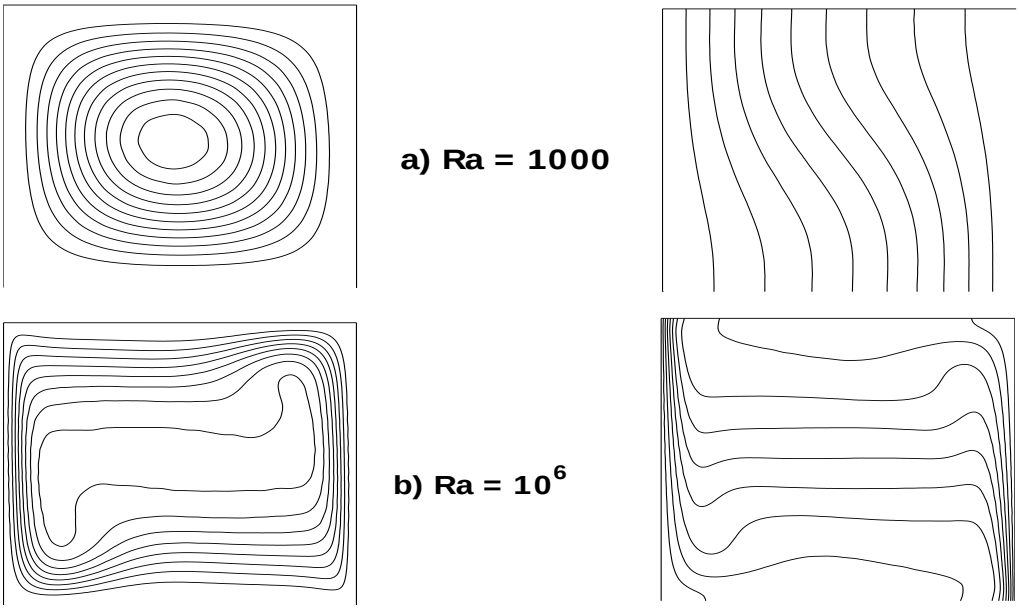

Fig. 2. Streamlines and isotherms A =1, φ = 90°, ZHF (Right side is the hot surface).

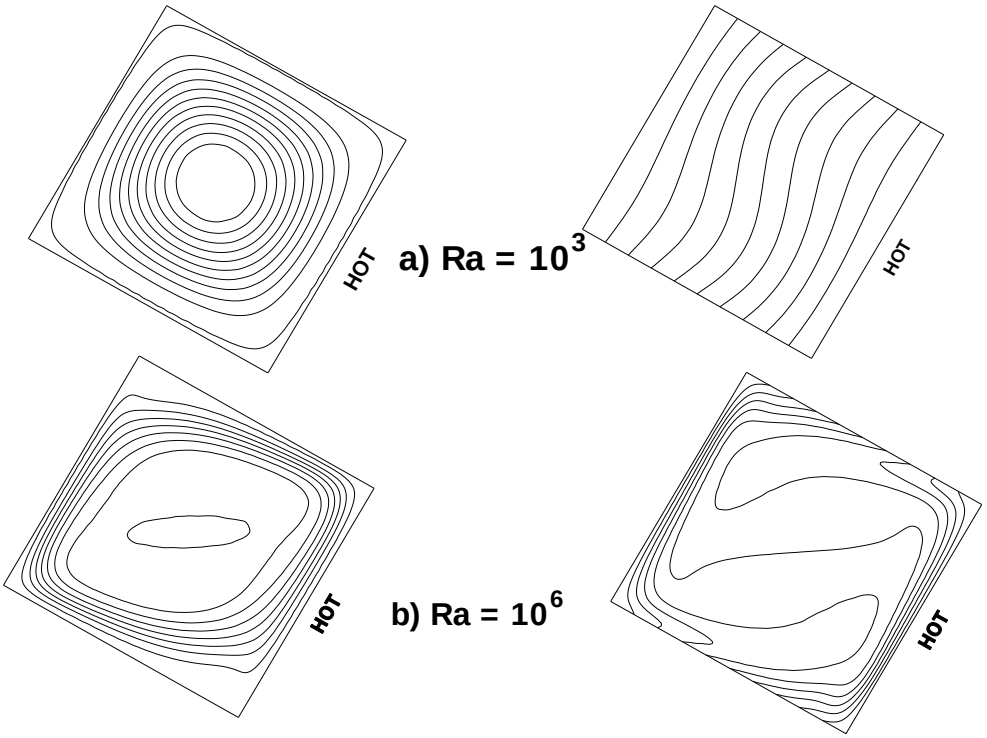

Fig. 3. Streamlines and isotherms A =1, φ = 60°, LTP (Right side is the hot surface).

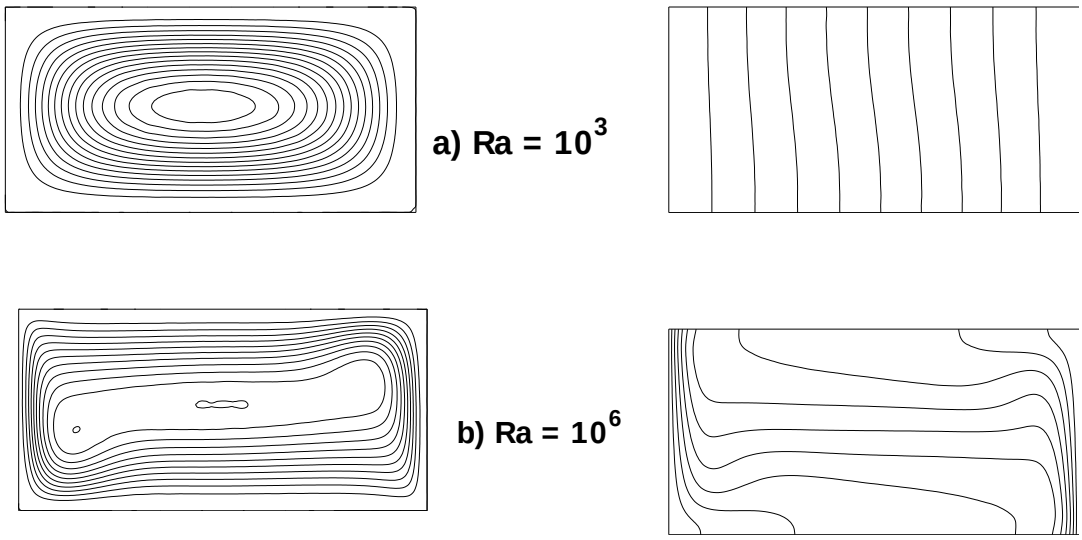

Fig. 4. Streamlines and isotherms A=0.5, φ = 90°, ZHF (Right side is the hot surface).

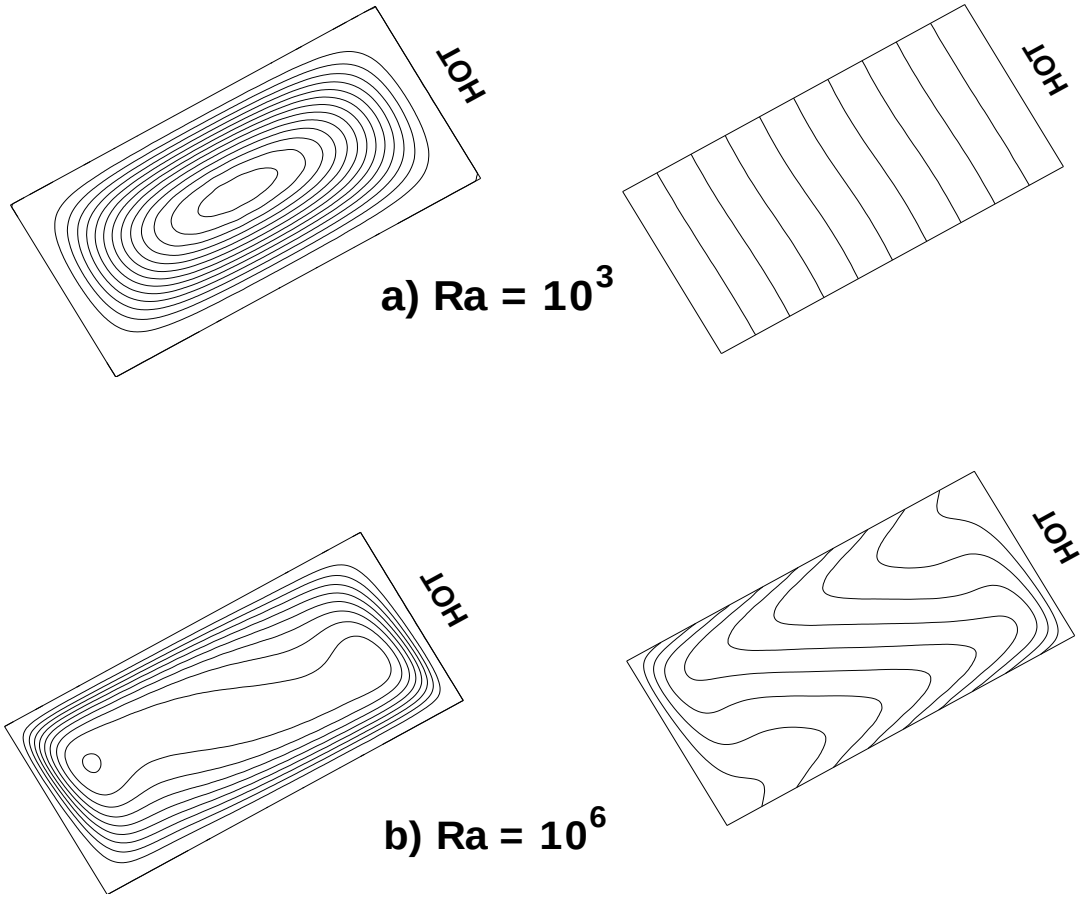

Fig. 5. Streamlines and isotherms A = 0.5, φ = 120°, LTP.

4.4. Local Nusselt number distribution

Fig. 9 shows the distribution of Nu_x on the hot surface for A = 1, φ = 90° and ZHF. The value of Nu_x increases with Ra and decreases up along the hot surface with a local maximum close to the bottom of the hot surface. The location of this maximum shifts closer to the lower end of the hot surface as Ra was increased.

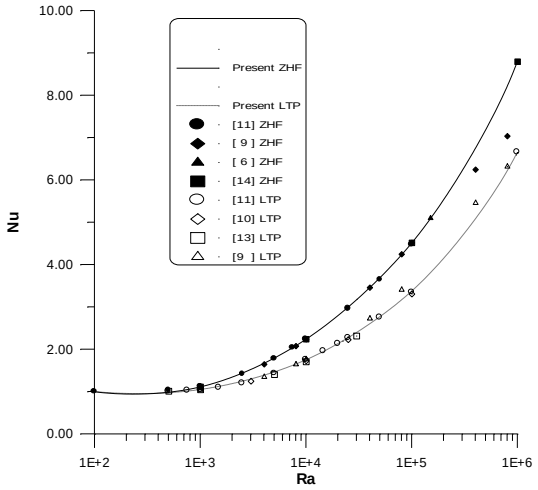

Fig. 6. Effect of side walls boundary conditions A = 1, φ = 90°.

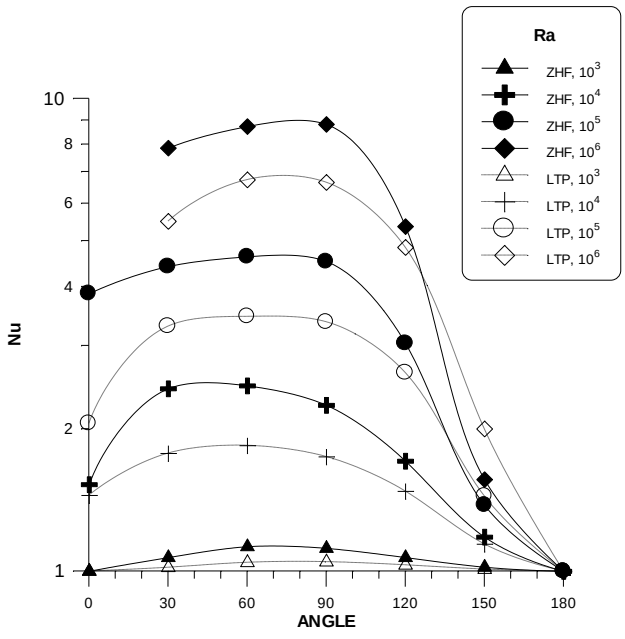

Fig. 7. Heat transfer data for A = 1.

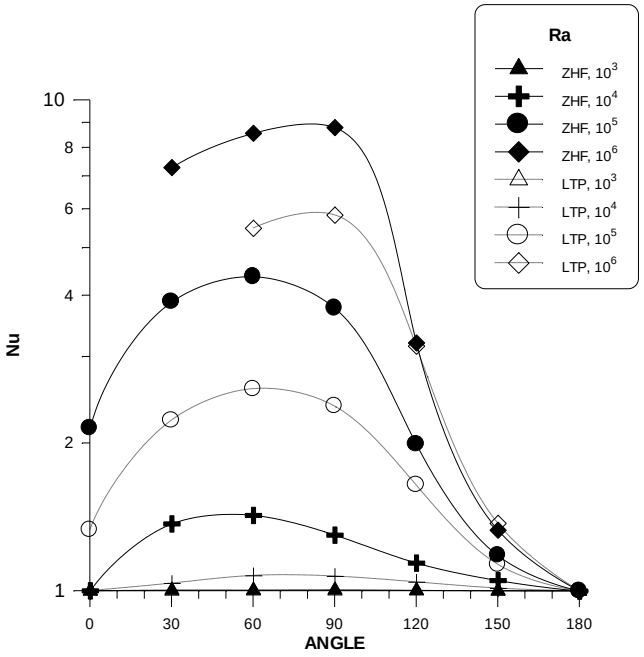

Fig. 8. Heat transfer data for A = 0.5.

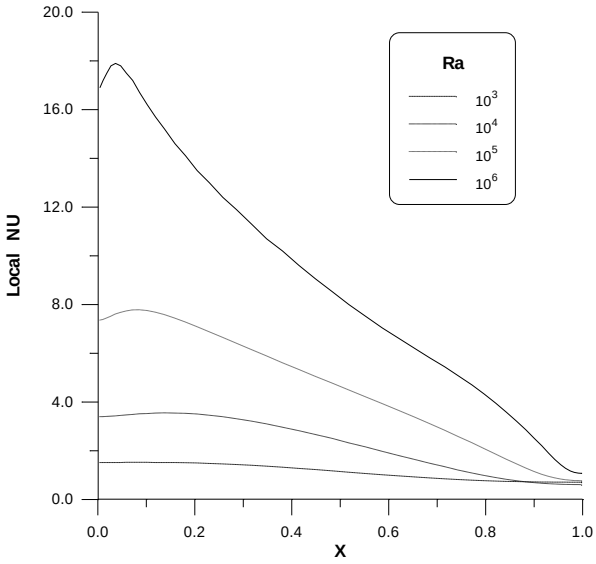

Fig. 9. Local Nu distribution on hot surface A = 1, φ = 90°, ZHF.

4.5. Temperature and velocity distributions

The dimensionless temperature distribution at the cavity mid plane (X = 0.5) is shown in fig. 10 for A = 1, φ = 90° and ZHF. For Ra = 10^3, the distribution is almost linear indicating the conduction regime. For $Ra \geq 10^4$, a constant temperature occurs in the core

of the cavity and a higher temperature slope occurs near the isothermal surfaces indicating the laminar boundary layer regime. As Ra increases, the temperature slope increases indicating higher heat transfer.

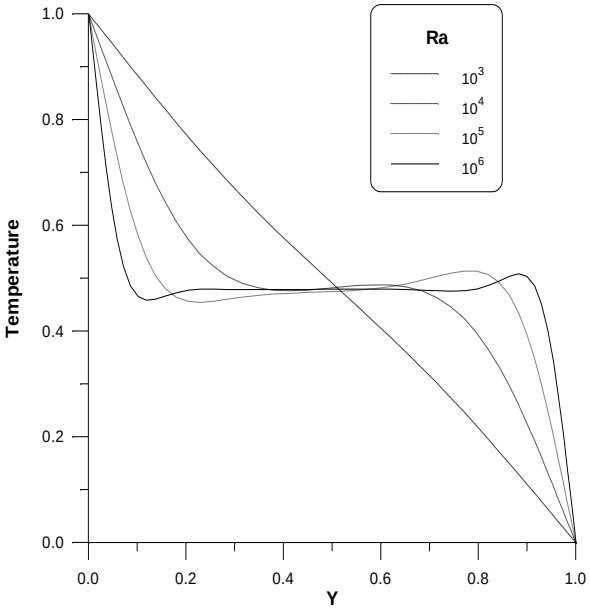

Fig. 10. Temperature distribution at $X = 0.5$, $A = 1$, $\varphi = 90°$, ZHF.

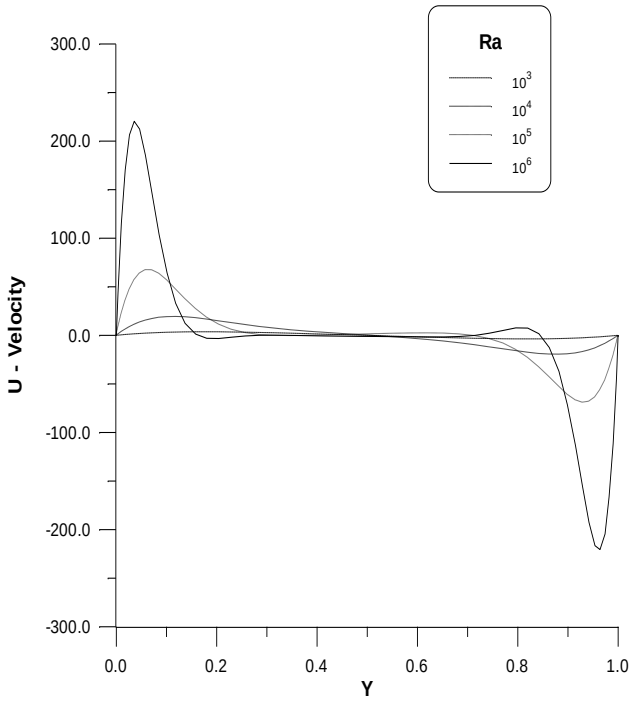

Fig. 11. U-Velocity distributions at X = 0.5, $A = 1$, $\varphi = 90°$, ZHF.

The distribution of the dimensionless velocity component U (in x - direction) is plotted in fig. 11 at mid plane for $A = 1$, $\varphi = 90°$ and ZHF. The velocity increases from the no-slip value (zero) at the hot surface to a local maximum and then decreases to almost zero value in the core, then it decreases to a local minimum close to the cold surface and again to the no-slip value at the surface. The local maximum and minimum increase in value and shift closer to the surfaces as Ra was increased.

5. Experimental results

Measurements of average Nusselt numbers are obtained at two different angles of inclination ($\varphi = 60°$ and $90°$) for $A = 1$, $10^2 \le Ra \le 1.7 \times 10^8$ and LTP. Fig. 13 shows the present numerical results along with the

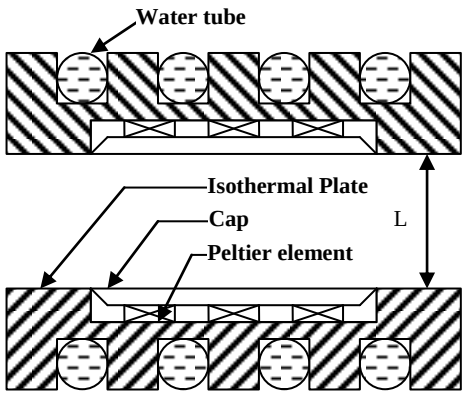

Fig. 12. Experimental setup.

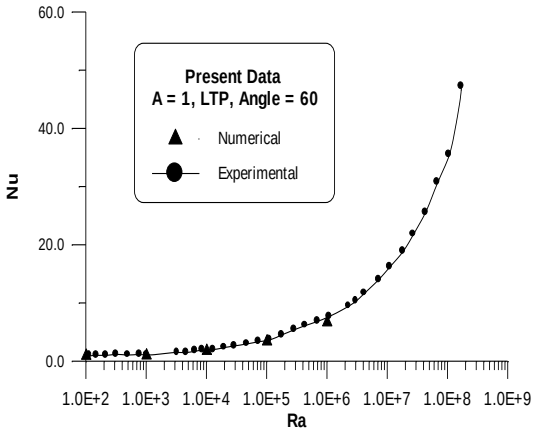

Fig. 13. Experimental and Numerical data $A = 1$, $\varphi = 60°$, LPT.

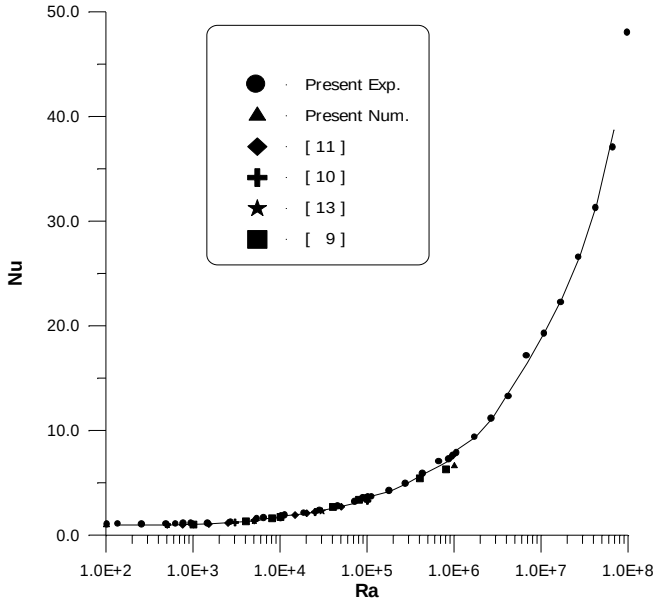

Fig. 14. Experimental and Numerical data $A = 1$, $\varphi = 90°$, LTP.

present experimental data. An excellent agreement is shown. A comparison of the present numerical and experimental data with previous published data for $A = 1$, $\varphi = 90°$ and LTP is given in fig. 14. The present experiments covered the conduction, laminar and turbulent boundary layer regimes. Excellent agreement with previous results is also noticed.

6. Conclusions

Numerical solutions to the steady state two-dimensional equations governing the flow in inclined rectangular air layers have been obtained. Several Rayleigh numbers and angles of tilt have been investigated for shallow layers of aspect ratios 1 and 0.50. and for both perfectly conducting and insulating side walls boundary conditions. The flow structure and heat transfer were strongly dependent on A, φ and Ra in a very complex way. The heat transfer is lower for LTP than for ZHF. The average Nu increased with Ra and decreased when A was lowered from 1 to 0.50. The case of heating from above ($\varphi > 90°$) gives lower Nu than that of heating from below ($\varphi < 90°$). Experimental results using the Peltier-effect for $A = 1$, $\varphi = 60°$ and 90° and for LTP were in excellent agreement with present and previous numerical and experimental data.

Nomenclature

A	is the cavity aspect ratio, H/L,
Cp	is the specific heat at constant pressure, $J/kg.K$,
g	is the gravitational acceleration, m/s^2,
Gr	is the Grashof number, $\beta g (T_h - T_c) L^3/\upsilon^2$,
h	is the average heat transfer coefficient, $W/m^2 K$
h_x	is the local heat transfer coefficient, W/m^2K,
H	is the cavity height, m,
k	is the fluid thermal conductivity, W/m.K,
k_w	is the wall thermal conductivity, W/m.K,
L	is the cavity width (plate spacing), m,
Nu	is the average Nusselt number, $h L/k$,
Nu_x	is the local Nusselt number, $h_x L/k$,
p_d	is the dynamic pressure, N/m^2,
P_d	is the dimensionless dynamic pressure,
Pr	is the Prandtl number, $Cp\ \mu/k$,
Ra	is the Rayleigh number, $\beta g(T_h - T_c) L^3/\alpha\upsilon$
T	is the temperature, K,
T_c	is the temperature of cold surface, K,
T_h	is the temperature of hot surface, K,
u	is the velocity in x-direction, m/s,
U	is the dimensionless velocity in x-direction,
υ	is the velocity in y-direction, m/s,
V	is the dimensionless velocity in y-direction,
x,y	are the Cartesian coordinates, and
X,Y	are the dimensionless coordinates.

Greek

α	is the thermal diffusivity, m^2/s,
β	is the volumetric coefficient of thermal expansion, 1/K,
θ	is the dimensionless temperature,

μ is the dynamic viscosity, kg/m.s,
υ is the kinematic viscosity, m^2/s,
ρ is the density, kg/m^3, and
φ is the angle of tilt from horizontal, rad.

References

[1] S. Ostrash, "Natural convection in Enclosures", J. Heat Transfer, Vol. 110, pp. 1175-1190 (1988).

[2] G.D. Raithby and K.G.T. Hollands, Handbook of Heat Transfer Fundamentals, Edited by W.M. Rohsenow, J.P. Hartnett and E.N. Ganic, McGraw-Hill, New York (1985).

[3] O. Aydin, A. Ünal and T. Ayhan, "Natural Convection in Rectangular Enclosures Heated from One Side and Cooled from the Ceiling", Int. J. Heat Mass Transfer, Vol. 42 (13), pp. 2345-2355 (1999).

[4] K.G.T. Hollands and L. Konicek, "Experimental Study of the Stability of Differentially Heated Inclined Air Layers", Int. J. Heat Mass Transfer, Vol. 16, pp. 1467-1476 (1973).

[5] I. N. Arnold, I. Catton and D.K. Edwards, "Experimental Investigation of Natural Convection in Inclined Rectangular Regions of Differing Aspect Ratios", J. Heat Transfer, Vol. 98, pp. 67-71 (1976).

[6] I.P. Jones, "A Numerical Study of Natural Convection in an Air-Filled Cavity: Comparison with Experiment", Num. Heat Transfer, Vol. 2, pp. 193-213 (1979).

[7] S.M. ElSherbiny, G.D. Raithby and K.G.T. Hollands, "Heat Transfer by Natural Convection Across Vertical and Inclined Air Layers", ASME Journal of Heat Transfer, Vol. 104, pp. 96-102 (1982).

[8] W.M.M. Schinkel, S.J.M. Linthorst and C.J. Hoogendoorn, "The Stratification in Natural Convection in Vertical Enclosures", J. Heat Transfer, Vol. 105, pp. 267-272 (1983).

[9] I. Catton, P.S. Ayyaswamy and R.M. Clever, "Natural Convection Flow in a Finite Rectangular Slot Arbitrarily Oriented with Respect to the Gravity Vector", Int. J. Heat Mass Transfer, Vol. 17, pp. 173-184 (1974).

[10] W. Koutsoheras and W.W.S. Charters, "Natural Convection Phenomena in Inclined Cells with Finite Side-Walls - A Numerical Solution", Solar Energy, Vol. 19, pp. 433-438 (1977).

[11] B. Roux, J.C. Grondin, P. Bontoux and B. Gilly, "On a High-Order Accurate Method for the Numerical Study of Natural Convection in a Vertical Square cavity", Num. Heat Transfer, Vol. 1, pp. 331-349 (1978).

[12] B.A. Meyer, J.W. Mitchell and M.M. El-Wakil, "Natural Convection Heat Transfer in Moderate Aspect Ratio Enclosures", J. Heat Transfer, Vol. 101, pp. 655-659 (1979).

[13] B.A. Meyer, J.W. Mitchell and M.M. El-Wakil, "The Effect of Thermal Wall Properties on Natural Convection in Inclined Rectangular Cells", J. Heat Transfer, Vol. 104, pp. 111-117 (1982).

[14] G. DeVahl Davis, "Natural Convection of Air in a Square Cavity: A Bench Mark Numerical Solution", Int. J. Numerical Methods in Fluids, Vol. 3, pp. 249-264 (1983).

[15] R. A. Kuyper, TH.H. Van der Meer, C.J. Hoogendoorn and R.A.W.M. Henkes, "Numerical Study of Laminar and Turbulent Natural Convection in an Inclined Square Cavity", Int. J. Heat Mass Transfer, Vol. 36 (11), pp. 2899-2911 (1993).

[16] N. Ramesh and S.P. Venkateshan, "Experimental Study of Natural Convection in a Square Enclosure Using differential interferometer", Int. J. Heat Mass Transfer, Vol. 44 (6), pp. 1107-1117 (2001).

[17] I. Catton, "The Effect of Insulating Vertical Walls on the Onset of Motion in a Fluid Heated from Below", Int. J. Heat Mass Transfer, Vol. 15, pp. 667-672 (1972).

[18] S.M. ElSherbiny, K.G.T. Hollands, and G.D. Raithby, "Effect of Thermal Boundary Conditions on Natural Convection in Vertical and Inclined Air Layers", ASME journal of Heat

Transfer, Vol. 104, pp. 515-520, (1982).

[19] S.V. Patankar, "Numerical Heat Transfer and Fluid Flow", Mc Graw-Hill, New York (1980).

[20] E.C. Shewen, "A Peltier-Effect Technique for Natural Convection Heat Flux Measurements Applied to the Rectangular Open Cavity", Ph. D. Thesis, University of Waterloo, Waterloo, Canada (1986).

Received August 16, 2004
Accepted September 13, 2004